

Dynamics of Quantum Analogs of Classical Impact Oscillators

Arnab Acharya*, Titir Mukherjee†, Deepshikha Singh‡, Soumitro Banerjee§

Abstract

This paper investigates the dynamics of quantum analogs of classical impact oscillators to explore how complex nonlinear behaviors manifest in quantum systems. While classical impact oscillators exhibit chaos and bifurcations, quantum systems, governed by linear equations, appear to forbid such dynamics. Through simulations of unforced, forced, and dissipative quantum oscillators, we uncover quasiperiodicity, strange nonchaotic dynamics, and even chaos in the presence of dissipation. Using entropy time series, Fourier spectra, OTOCs, Lyapunov analysis, and the 0–1 test, we demonstrate that quantum systems can exhibit rich dynamical signatures analogous to classical nonlinear systems, bridging quantum mechanics and chaos theory.

1 Introduction

It is known that classical nonlinear systems can exhibit an array of complex dynamical behaviors, including limit cycles, quasiperiodicity, strange nonchaotic orbits, and chaos. In contrast, it is believed that quantum systems cannot exhibit such dynamics because of their linear nature. This poses a fascinating puzzle: If the classical world emerges from the quantum world, how can complex dynamical behaviors emerge? After all, classical systems are built on quantum systems at a fundamental level! To probe this issue, we ask: What dynamical phenomena can a quantum system exhibit?

The field of quantum chaos seeks to answer this question by identifying the quantum signatures (mainly in terms of the distribution of energy levels) in systems whose classical counterparts are chaotic Stöckmann (1999); Haake (1991); Cvitanovic *et al.* (2020). For example, Bohigas *et al.* (1984) conjectured that the energy level statistics of a classically chaotic quantum system follow the predictions of random matrix theory (RMT). While trying to explain the spectra of complex nuclei, Eugene Wigner came up with the idea of representing the Hamiltonian with a Hermitian matrix whose elements are drawn randomly from a normal distribution. Subsequently, this approach has led to successful predictions regarding the statistics of eigenvalues of complex quantum systems.

It has been found that in systems whose classical limits are not chaotic, the eigenvalues are uncorrelated, and their spacings follow the Poisson distribution ($P(s) \sim e^{-s}$, where s is the normalized level spacing). In systems with a chaotic classical limit, the spacings of the energy levels follow either the Gaussian Unitary Ensemble (GUE), the Gaussian Orthogonal Ensemble (GOE), or the Gaussian Symplectic Ensemble (GSE) Mehta (2004) depending on the symmetries of the system. When the system has no symmetries, the Hamiltonian is a Hermitian matrix with complex entries, and the GUE statistics are followed. If the system has time-reversal symmetry, the matrices are real-valued symmetric, and GOE is followed. For time-reversal symmetric systems with rotational/spin symmetries, the matrices have quaternionic entries, and

*dr.arnab.acharya@gmail.com

†tm21rs050@iiserkol.ac.in

‡ds21ms133@iiserkol.ac.in

§Corresponding author, soumitro@iiserkol.ac.in

Department of Physical Sciences, Indian Institute of Science Education & Research, Kolkata, India

GSE is followed. Each ensemble has characteristic level spacing statistics: for GOE, $P(s) = \frac{\pi s}{2} \exp\left(-\frac{\pi s^2}{4}\right)$; for GUE, $P(s) = \frac{32s^2}{\pi^2} \exp\left(-\frac{4s^2}{\pi}\right)$; and for GSE, $P(s) = \frac{2^{18}}{3^6\pi^3} s^4 \exp\left(-\frac{64s^2}{9\pi}\right)$.

Additionally, there is a deep connection between the classical unstable periodic orbits of chaotic systems and the quantum density of states (energy spectrum in the case of bound states) Gutzwiller (2013). Another prominent connection is the presence of anomalously high probability densities along certain unstable classical periodic orbits, called quantum scars Heller (1984); Kaplan & Heller (1999).

In our work, we adopt a different route. The ‘state’ of a quantum system is represented by the wavefunction $\Psi(x, t)$, a complex-valued function of space and time. The system dynamics would be given by the evolution of the wavefunction following the Schrödinger equation. We try to infer the qualitative character of the system dynamics from the oscillation of the wavefunction.

Any study requires a model system. For our purpose, it needs to be a simple classical system whose quantum analog can be easily constructed. We chose the impact oscillator as our model because it is a very simple mechanical system that exhibits rich dynamics due to grazing-induced bifurcations Nordmark (1991a); Chin *et al.* (1994); di Bernardo *et al.* (2008).

In order to apply the established methods of nonlinear dynamics, we need to convert the dynamics of the complex-valued wavefunction into a real-valued time series. This can be achieved by using the expectation values of the observables Shankar (2012), the autocorrelation function Nauenberg (1990), the L_1 -norm Horn & Johnson (1985), and quantum entropies Chegade & Vershynina (2019). After trying various possibilities, we decided to use the entropy to generate a real-valued time series because of its suitability to distinguish qualitatively different types of dynamics.

In classical dynamics, Takens’ embedding theorem allows us to reconstruct the phase space of a system from a single time series. Although a direct quantum analog is not straightforward, we can visualize quantum dynamics in a phase-space-like representation using quasiprobability distributions. The most famous of these is the Wigner function, $W(x, p)$, which provides a ‘quantum phase space portrait’ of the system. Although it is not a true probability distribution (it can take on negative values, a clear sign of quantum interference), its evolution can reveal important dynamical features. Studies have shown that the structure of the Wigner function can reflect the underlying classical dynamics, with quantum interference effects becoming more pronounced in chaotic systems and it can also exhibit ‘scars’ (Heller, 1984).

The Lyapunov exponent (LE), which quantifies the rate of exponential divergence of classical trajectories, has a quantum counterpart in the form of an out-of-time-order correlator (OTOC). The OTOC, defined as

$$C(t) \equiv -\langle [\widehat{W}(t), \widehat{V}(0)]^2 \rangle, \quad (1)$$

measures how a small local perturbation affects a later measurement. Here, $\widehat{V}(0)$ and $\widehat{W}(t)$ are two Hermitian operators in the Heisenberg picture at times 0 and t , and the brackets $\langle \cdot \rangle$ represent either a quantum-mechanical expectation value or a thermal average, depending on the context Hashimoto *et al.* (2017). In a system with periodic dynamics, the OTOC varies periodically or quasiperiodically with time Hashimoto *et al.* (2017); Li *et al.* (2023). In quasiperiodically driven systems, the OTOC exhibits power-law growth at early times, as observed in the Aubry–André model Riddell & Sørensen (2020). In systems where OTOC grows exponentially in time as $C(t) \sim e^{\lambda_L t}$ before saturating, the dynamics is typically considered chaotic Akutagawa *et al.* (2020).

Another method of distinguishing different types of dynamics is to analyze the frequency spectrum. A periodic orbit is expected to have a fundamental component and its harmonics; a quasiperiodic orbit is supposed to have more than one fundamental frequency and combinations of their harmonics; a strange nonchaotic orbit has dense but discrete peaks in the spectrum Prasad *et al.* (2001); and a chaotic orbit has a spread spectrum—a continuum of frequency components Huberman & Zisook (1981).

The 0-1 test Gottwald & Melbourne (2004) has been proposed as a reliable method of distinguishing between chaotic and nonchaotic time series. It takes a sampled data set as input and outputs a single value, K , between 0 and 1, with 0 indicating periodicity/quasi-periodicity and 1 indicating chaos. No prior information about the system is required to apply the test. This test proved to be particularly useful in our case, as the entropy time series is all we have to diagnose the qualitative character of the system.

Bifurcation diagrams are a staple of nonlinear dynamics, illustrating how a system’s behavior changes as a parameter is varied. Although the linearity of the Schrödinger equation prevents true bifurcations in the classical sense, analogous phenomena can be observed in quantum systems through parameter-dependent changes in their properties. By systematically changing a parameter in a quantum system (like the strength of a driving field), we can observe abrupt changes in the system’s properties, such as its energy level structure or the morphology of its wavefunctions. These transitions, often termed quantum bifurcations, can be visualized in diagrams that bear a striking resemblance to their classical counterparts. For example, studies of molecular systems have shown how nonadiabatic couplings can lead to ‘bifurcation’ and merging of quantum wave packets, inducing complex dynamics (Takami & Fujisaki, 2024).

Earlier studies on the classical impact oscillator considered a friction or dissipative element and demonstrated an abrupt transition to chaos at grazing Nordmark (1991b); di Bernardo *et al.* (2008); Banerjee *et al.* (2009). In quantum mechanics, dissipation is typically addressed by modeling the system as open, i.e., interacting with an external environment or bath. This bath is often represented as a collection of harmonic oscillators. Such a framework enables researchers to explore how the dynamical properties evolve in the presence of decoherence and energy loss.

In recent years, the study of quantum chaos in dissipative settings has shown that dissipation, while suppressing coherence, can also sustain chaotic signatures for longer durations Roy & Bhattacharjee (2025), as demonstrated in many-body systems where chaos is linked to decoherence, entanglement, and thermalization Nayak & Das (2025); Lee & Wang (2024). Classical chaotic systems such as the kicked top Chaudhury & et al. (2014); Haake *et al.* (1987), Duffing oscillator Kumar & Paul (2023); Singh & Mehta (2021), and the Morse oscillator Korsch & Laurent (1987) have long served as benchmarks for exploring the correspondence between classical and quantum in dissipation. However, in comparison, the soft impact oscillator—despite being a canonical piecewise-smooth system in the classical domain—has received relatively little attention in the quantum dissipative regime, motivating the present study.

The standard framework for studying open quantum systems is the Lindblad master equation Manzano (2020); Nafari Qaleh & Rezakhani (2022), which is based on the construction of suitable jump operators to represent environmental effects. While this works well for systems with certain symmetries, it becomes impractical for cases like the quantum impact oscillator, where the lack of symmetry leads to an infinite and computationally expensive expansion.

To overcome these challenges, we adopt the quantum Langevin equation (QLE) formalism, which offers a tractable alternative for modeling dissipative dynamics in open quantum systems. We consider a system coupled to a bath of harmonic oscillators and, following standard procedures Ford *et al.* (1988); Agarwal (1971), transition to the Heisenberg picture. By deriving the equations of motion for both system and bath operators and subsequently eliminating the bath degrees of freedom, we obtain an effective description of the dynamics of the system.

We employ all of the above methods to analyze the dynamics of the quantum system. The paper is organized as follows. In Section 2, we introduce the classical impact oscillator and its quantum analog. In Section 3 we analyze the dynamics of the quantum impact oscillator and show that in the absence of forcing and dissipation it shows quasi-periodic motion. In Section 4 we analyze the system behavior in the presence of sinusoidal forcing and show that it can exhibit strange nonchaotic behavior. In Section 5 we study the behavior of the system with dissipation as an open quantum system using the quantum Langevin equation and show that it can exhibit

chaotic behavior. In Section 6 we conclude.

2 The impact oscillator

In order to investigate whether quantum systems can manifest complex dynamics, we consider the quantum analog of a classical system, the impact oscillator.

2.1 The Classical Impact Oscillator

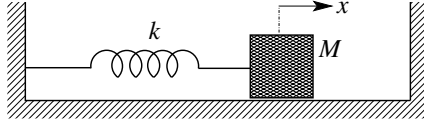


Figure 1: Schematic diagram of a simple impact oscillator.

The system consists of a mass-spring arrangement in which the mass can collide with a rigid wall (schematic shown in Fig. 1). In the absence of any external forcing, the potential function is described by:

$$V(x) = \begin{cases} \frac{1}{2}kx^2 & \text{if } x < x_w \\ \infty & \text{if } x \geq x_w \end{cases} \quad (2)$$

where x is the deviation from the relaxed position of the spring and x_w is the position of the wall.

For this system, each trajectory in the phase space is periodic, with the *grazing* orbit dividing the phase space into two dynamically distinct regions (Fig. 2).

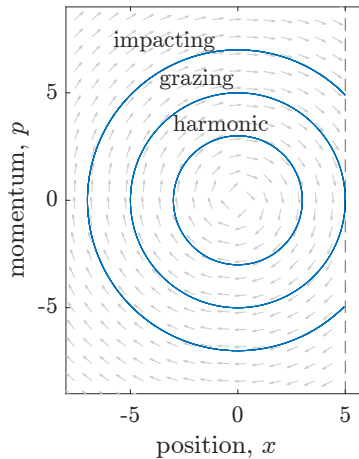


Figure 2: Phase space trajectories of the simple impact oscillator.

2.2 Quantum Impact Oscillator

The quantum analog of this system would be a particle confined by the same potential function (2) as shown in Fig. 3. The dynamics of the particle would be given by the evolution of the wavefunction $\Psi(x, t)$ following the Schrödinger equation

$$i\hbar \frac{\partial}{\partial t} \Psi(x, t) = \left(-\frac{\hbar^2}{2m} \frac{d^2}{dx^2} + V(x) \right) \Psi(x, t). \quad (3)$$

The parameters were taken as $k = 1$, $m = 1$. We have used natural units with $\hbar = 1$. There are several techniques to numerically solve the Schrödinger equation. We have used the

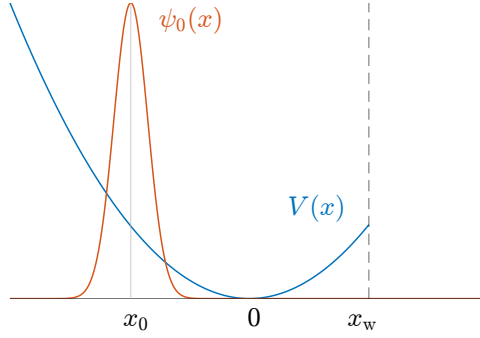


Figure 3: The impact oscillator potential (blue) with a Gaussian wavepacket (red) as the initial condition.

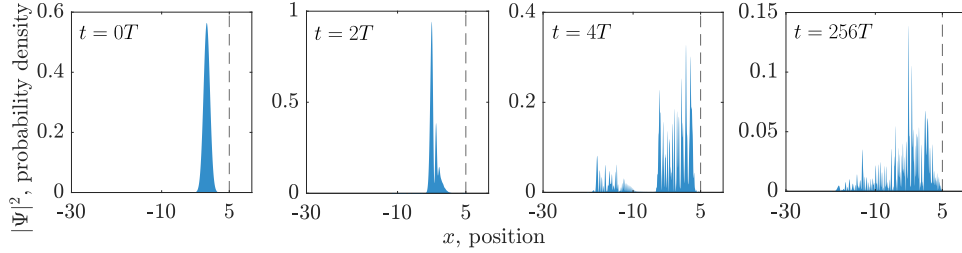


Figure 4: Snapshots of the evolution of the probability density function for the grazing initial conditions with $A_f = 3.0905$ $T = 2\pi/\omega_f$ is one time period of the forcing.

Numerov-Cooley scheme Numerov (1933); Cooley (1961) and the results were verified by direct diagonalization of the Hamiltonian matrix Izaac & Wang (2018).

The simulation starts from an initial condition, and in the quantum system, it would be the initial wavefunction. We choose a Gaussian wavepacket with variance $\frac{\hbar}{2\sqrt{km}}$ that has a minimum uncertainty, and shift the mean position to $x = -5$, which is equivalent to releasing the mass from a stressed position of the spring corresponding to the classical grazing condition ($x_w = 5$).

3 Dynamics of the quantum impact oscillator

For the quantum impact oscillator, when the wall is placed far away, the dynamics of the wavefunction is similar to that of a harmonic oscillator (it oscillates periodically around the mean position). But it becomes aperiodic as the wall approaches the classical grazing condition. A way of representing the dynamics of a quantum system in the phase space is provided by the Wigner distribution function:

$$W(x, p) = \frac{1}{\pi\hbar} \int_{-\infty}^{\infty} \Psi^*(x+y) \Psi(x-y) e^{2ipy/\hbar} dy \quad (4)$$

It gives a quasi-probability distribution over the phase space. We found that near the grazing condition, the Wigner distribution evolves aperiodically with definite patterns. Fig. 5 shows a snapshot of the evolving distribution. The occurrence of negative values, implying non-classical behavior, is noticeable.

In order to find out the qualitative character of the dynamics, we need to convert the dynamics of the complex-valued wavefunction into a real-valued time series. The entropy of the

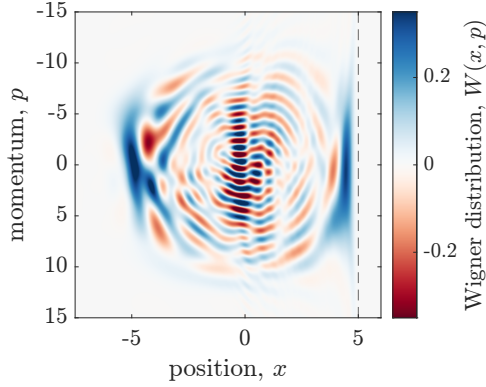


Figure 5: A snapshot of the evolving Wigner distribution for the grazing condition at $t = 100$.

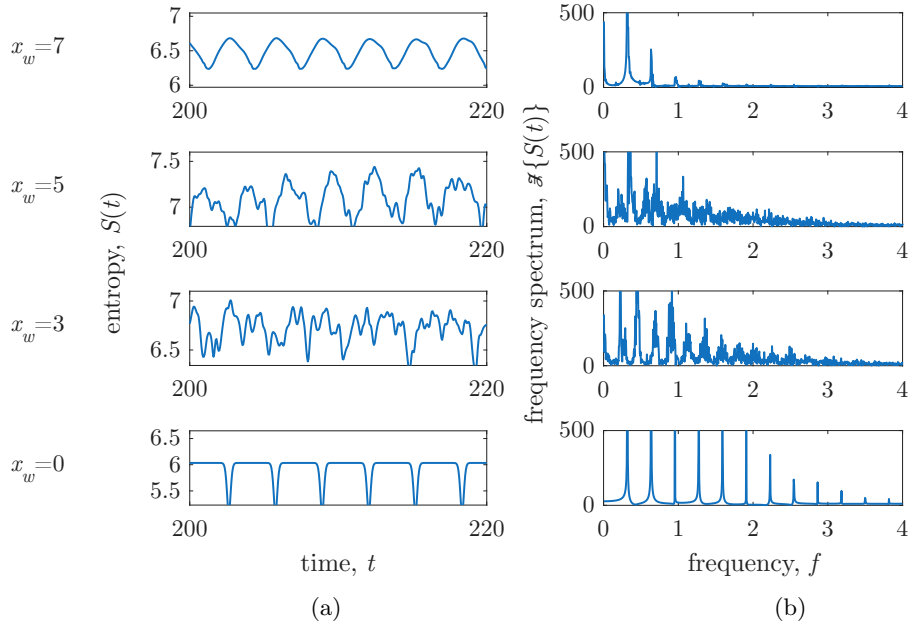


Figure 6: (a) Entropy of the probability density $|\psi(t)|^2$ versus time for different wall positions. (b) Frequency spectrum of the entropy time-series.

probability density (Shannon, 1948)

$$S(t) = - \int |\Psi(x, t)|^2 \log(|\Psi(x, t)|^2) dx \quad (5)$$

generates such a time series (see Fig. 6a). It shows that when the wall is far away the behavior is periodic. As the wall is moved closer ($x_w = 6$), the waveform becomes aperiodic. In the classical grazing condition ($x_w = 5$), the aperiodic nature is quite pronounced. When the wall is moved to the middle of the potential function, i.e., when the system is a ‘half-harmonic oscillator’ ($x_w = 0$), the waveform is again periodic.

Fig. 6b shows the frequency spectrum of this time series. It shows an increasing number of discrete peaks as the wall approaches the grazing condition, indicating a complex quasiperiodic motion. This behavior contrasts sharply with that of the classical system, which remains periodic for all wall positions.

When the time series corresponding to different wall positions were subjected to the 0-1 test Gottwald & Melbourne (2004), they returned values close to zero, indicating that the visible aperiodicity in the time series is due to quasiperiodicity rather than chaos. This result is consistent with the linear nature of quantum evolution.

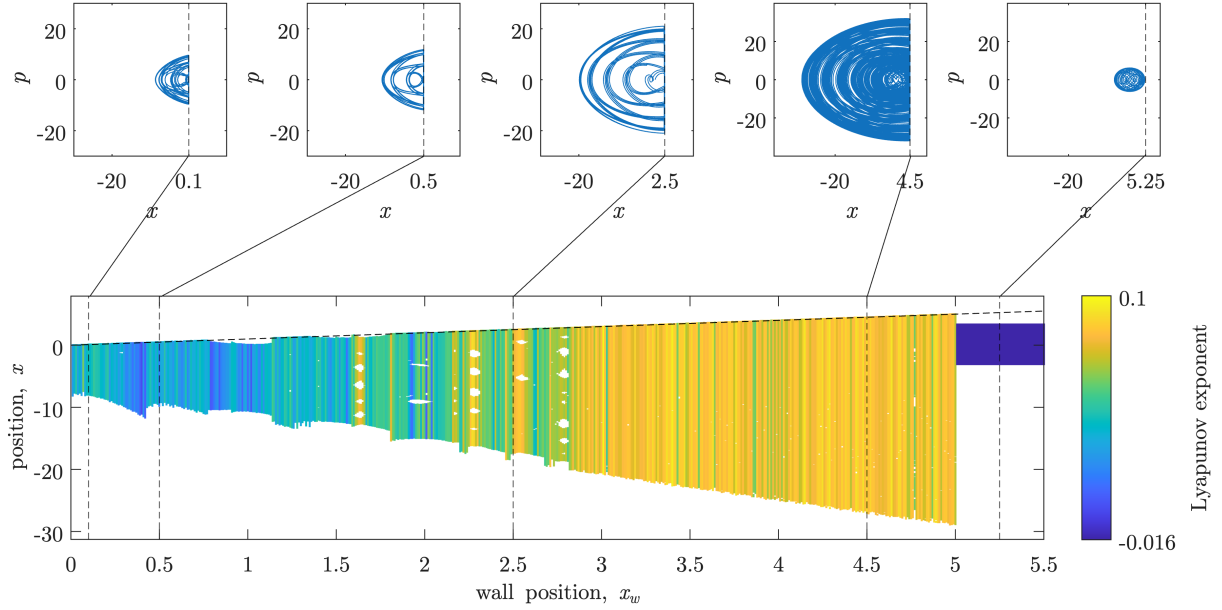


Figure 7: Bifurcation diagram of the classical forced impact oscillator as a function of wall position. Color indicates the maximal Lyapunov exponent.

4 The impact oscillator with forcing

When sinusoidal forcing $f(t) = A_f \sin(\omega_f t)$ is applied to the mass, the classical impact oscillator shows (Fig. 7) a sudden transition to a chaotic oscillation of large amplitude when the mass grazes the wall (Nordmark, 1991a; Ing *et al.*, 2008; di Bernardo *et al.*, 2008). The system exhibits windows of chaos, quasiperiodicity, and periodicity depending on the wall position and forcing parameters.

4.1 The quantum analog with forcing

In this case, the evolution of the wavefunction is given by the same Schrödinger equation (3), with the potential function changed to

$$V(x) = \begin{cases} \frac{1}{2}kx^2 + x A_f \sin(\omega_f t) & \text{if } x < x_w \\ \infty & \text{if } x \geq x_w \end{cases} \quad (6)$$

Solving the Schrödinger equation for a time-dependent Hamiltonian is a critical task in quantum mechanics. We adopt the Commutator-free Exponential Time-Propagators (CFETs) method Alvermann & Fehske (2011) to solve this system, which is outlined in Appendix A.

4.2 Dynamics of the quantum analog

What are the behaviors exhibited by the forced impact oscillator in the quantum regime?

The initial state is assumed to be a Gaussian wavepacket with mean at $x = 0$ and variance $\hbar/(2\sqrt{km})$. The natural frequency of the harmonic oscillator without the wall is 1, and the forcing frequency is considered an irrational number $(\sqrt{5} + 1)/2$.

Upon solving the equation numerically, we found that the forced quantum impact oscillator reveals more exotic behavior (Fig. 8a). As the wavefunction is an extended entity in space, the grazing condition cannot be defined as in the classical case. To find the grazing condition, we remove the wall and observe the dynamics of the coherent state in the (now) harmonic potential subjected to the same sinusoidal driving. We allow the time evolution to reach a steady state of oscillation. The condition for which the peak of the probability distribution $|\Psi|^2$

just reaches the position where the wall would have been, is taken to be the grazing condition for the quantum impact oscillator. For $x_w = 5$ and $\omega_f = (\sqrt{5} + 1)/2$, we find the condition for grazing as $A_f = x_w m \omega_0 |\omega_f - \omega_0| \approx 3.09$ where $\omega_0 = \sqrt{k/m}$ is the natural frequency. In subsequent simulations, this value of A_f has been set, so $x_w = 5$ can be taken as the grazing condition.

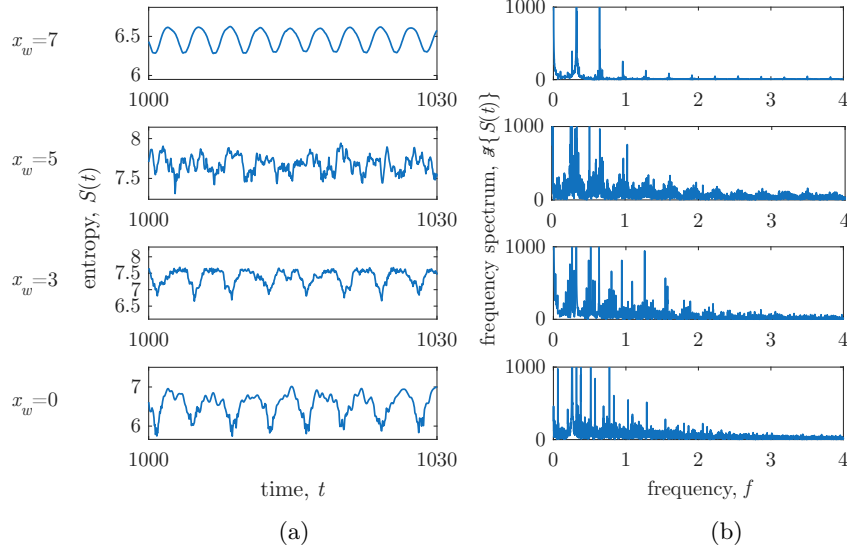


Figure 8: (a) Time-series of the entropy of the probability distribution. (b) Fourier spectra of the entropy time-series for different positions of the wall.

We notice the following aspects. These were first reported in Acharya *et al.* (2023); here we report the results obtained using the more accurate CFETs algorithm.

Dense discrete spectrum: The Fourier spectrum of the entropy time series (Fig. 8b) shows that, as the wall position approaches the grazing condition, a large number of discrete peaks appear. Repeated zooms of the spectrum shown in Fig. 9 reveal a dense set of discrete frequency peaks. This could be indication of a spectrum with fractal character (singular continuous spectrum). It has been shown (Bezhaeva & Oseledets, 1996) that the appearance of a dense discrete spectrum is a characteristic of strange nonchaotic orbits.

Power-law character in the spectral distribution function: To further investigate the issue, we obtain the spectral distribution function $N(\sigma)$: the number of frequency components above a threshold σ . Earlier research (Pikovsky & Feudel, 1995; Prasad *et al.*, 2001) has shown that, if the time series comes from a strange non-chaotic orbit, then the $N(\sigma)$ versus σ plot would show a power-law scaling. To verify, we plot $N(\sigma)$ versus σ in log-log scale (Fig. 10a). We find that it exhibits power-law scaling with an exponent of -2 .

Local instabilities: It is known that, even though the largest Lyapunov exponent for a strange non-chaotic orbit is negative, the dynamics can be locally unstable. This is captured by the finite-time Lyapunov exponents (Grassberger *et al.*, 1988; Kapitaniak, 1995). For the quantum forced impact oscillator, the distribution of finite-time Lyapunov exponents (Fig. 10 (b)) includes positive values, indicating local instability despite the globally non-chaotic nature (Prasad & Ramaswamy, 1999).

OTOC: We compute the out-of-time-order correlator (OTOC) using the method described in Hashimoto *et al.* (2017). The OTOC, defined by (1), is a quantity that helps track how quickly small perturbations spread through a quantum system over time. We take the two

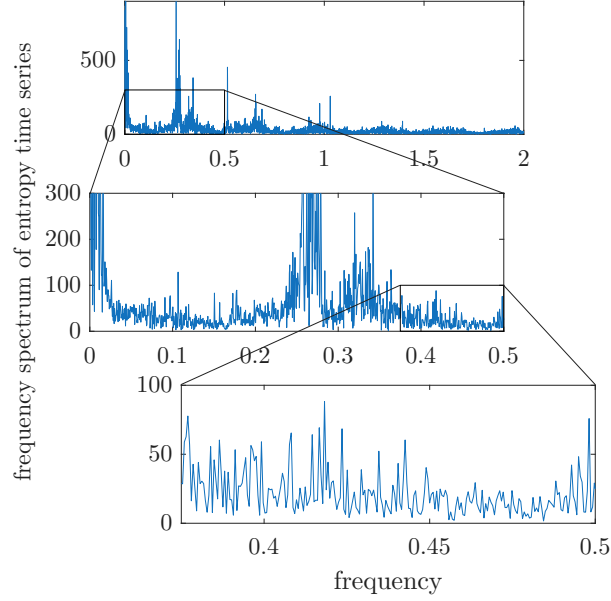


Figure 9: Two consecutive zooms of the frequency plot corresponding to Fig. 8, the case of $x_w = 5$.

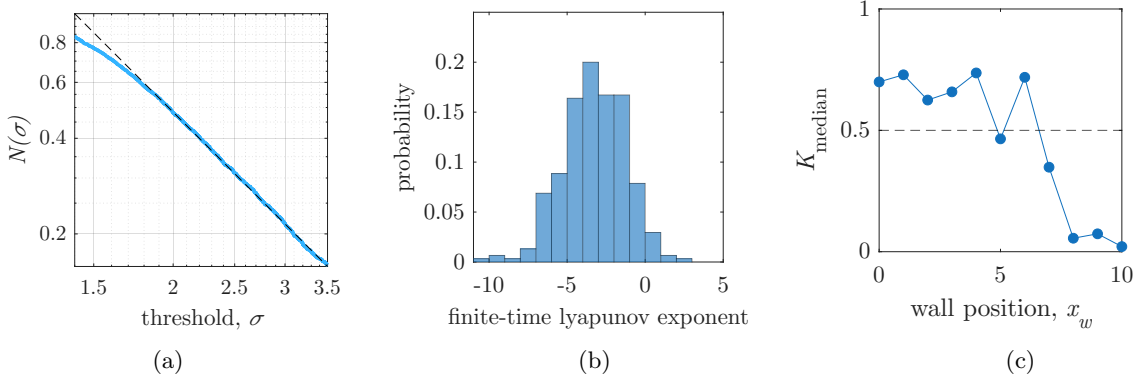


Figure 10: (a) Spectral distribution function, i.e., the number of peaks above threshold σ versus the threshold for the frequency spectrum of the entropy time-series for the forced quantum impact oscillator in log-log scale. (b) Distribution of finite-time Lyapunov exponents of the entropy time-series. Presence of positive parts indicates fractal structure of the underlying dynamics. (c) The variation of K_{median} , the metric from the modified 0-1 test, as the wall position is varied.

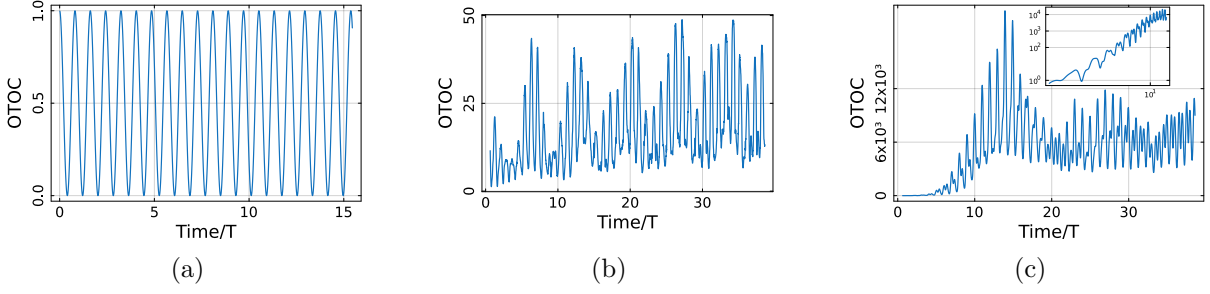


Figure 11: OTOC temporal behavior for $\beta = 0.5$ at three different wall positions: (a) $x_w = \infty$ (harmonic case), (b) $x_w = 1.2$, and (c) $x_w = 5.0$. Panel (a) shows periodic behavior, (b) displays a slow increasing trend, and (c) exhibits initial power-law growth followed by saturation. The inset in (c) confirms the power-law growth via a log-log plot. T refers time period of forcing.

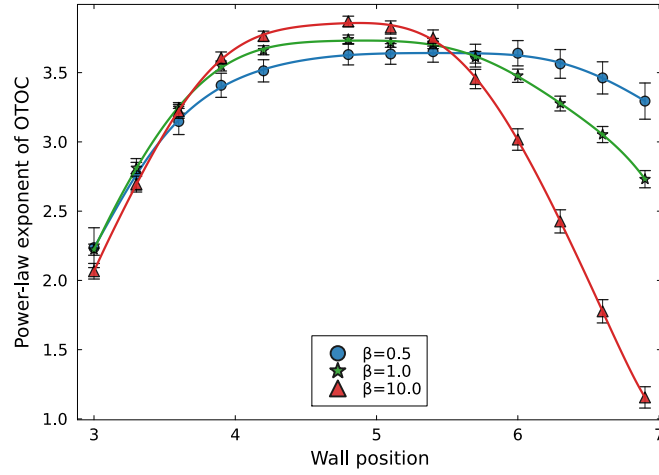


Figure 12: Power-law exponent of initial OTOC growth with respect to wall position x_w for three different temperatures $\beta = 0.5, 1.0, 10.0$. A polynomial fit has been used to estimate the trend. $\beta = 0.5$ is shown in blue with circle marker, $\beta = 1.0$ in green with star marker, and $\beta = 10.0$ in orange with triangle marker. The error bars correspond to the standard error when fitting the initial OTOC growth with a power-law.

operators as $x(t)$ and $p(0)$ in Heisenberg's picture (the position and momentum operators at times t and 0) so that the OTOC becomes $C_T(t) = -\langle [x(t), p(0)]^2 \rangle$, where the brackets $\langle \cdot \rangle$ represent a thermal or quantum average.

To make this more concrete, we express the thermal OTOC using the energy eigenstates of the system:

$$C_T(t) = \frac{1}{Z} \sum_n e^{-\beta E_n} c_n(t), \quad \text{with } c_n(t) \equiv -\langle n | [x(t), p]^2 | n \rangle, \quad (7)$$

where Z is the partition function, $\beta = \frac{1}{k_B T}$ represents the inverse temperature as we consider $k_B = 1$, and E_n and $|n\rangle$ are the energy eigenvalues and eigenstates of the system's time-independent Hamiltonian.

We evaluate the OTOC for different positions of the wall, x_w , ranging from 0 to 10 and ∞ , using 600 eigenstates at various inverse temperatures ($\beta = 0.5, 1.0$, and 10.0), with forcing amplitude $A_f = 3.0905$ and frequency $\omega_f = (\sqrt{5} + 1)/2$. For the harmonic case

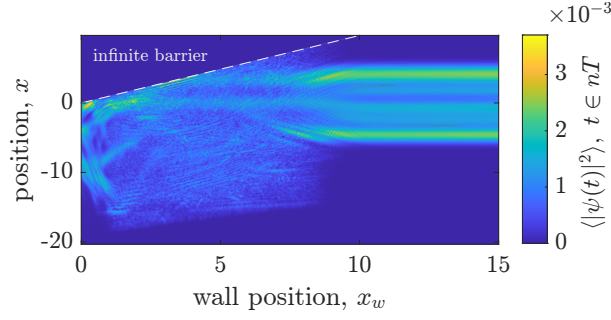


Figure 13: The quantum bifurcation diagram for the forced impacting system.

($x_w = \infty$), the OTOC remains periodic with significantly low amplitude (see Fig. 11a). In contrast, for $x_w = 0$ to 3.0, it shows a slight increasing trend (Fig. 11b).

For near-grazing impacts ($3.0 < x_w < 7.0$), the OTOC exhibits an initial power-law growth followed by saturation and bounded oscillations (Fig. 11c), similar to behavior reported in quasiperiodically driven systems such as the Aubry–André model Riddell & Sørensen (2020) and also other non-chaotic systems such as the Ising Floquet system Shukla *et al.* (2022). We fit the early-time OTOC growth to a power-law across the wall positions for the chosen temperatures. The exponent, quantifying the rate of information scrambling, increases with x_w approaching grazing conditions and then decreases. This peak shifts to smaller x_w as temperature is lowered (i.e., higher β) (see Fig. 12). Notably, we do not observe any exponential growth, confirming the absence of quantum chaos despite the presence of grazing impact.

0-1 test: It is known that, in a 0-1 test, a strange non-chaotic time series returns intermediate values between 0 and 1 (Kim, 2014; Gopal *et al.*, 2013). A few modifications of the 0-1 test make it more reliable for identification of strange non-chaotic dynamics, viz. addition of a small noise term Dawes & Freeland (2008), and fixing the value of c (a randomly chosen value in the original 0-1 test to prevent resonances) to suitable irrational numbers Gopal *et al.* (2013). For the quantum system, the modified 0-1 test applied to the entropy time series at the grazing condition yielded $K_{\text{median}} = 0.46$, indicating strange non-chaotic dynamics (Fig. 10(c)).

Bifurcation diagram: We plot the quantum bifurcation diagram by taking stroboscopic snapshots of the quantum probability density function and averaging it over a considerable number of periods. What we obtain is a distribution where the particle is more likely to be found. Then we plot this distribution, using color to represent high and low values, against a parameter, the wall position in our case. The quantum bifurcation diagram (Fig. 13) shows a dramatic increase in the complexity of probability density patterns around the grazing condition, reminiscent of the large-amplitude chaotic orbits in the classical system.

Based on the above observations, we conclude that the quantum forced harmonic oscillator exhibits strange nonchaotic dynamics close to the grazing condition.

5 The quantum forced impact oscillator with dissipation

To model the system with dissipation, we use the quantum Langevin equation. Specifically, we use the semiclassical formalism developed in Barik *et al.* (2003); Banerjee *et al.* (2004), which

enables us to work with the quantum expectation values of position and momentum, along with their fluctuations. A brief description of the method is given in Appendix B.

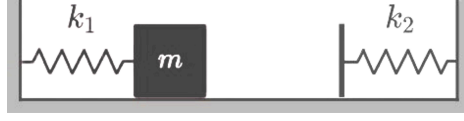


Figure 14: Schematic diagram of a soft impact oscillator

In the hard-impact oscillator, the potential function (2) has a derivative discontinuity, which causes all subsequent derivatives to be discontinuous. Since such terms appear in the model (see eqn. 19), this model cannot be used.

To address this, we consider a soft impact oscillator, where the rigid wall is replaced by a stiff, yet smooth, spring-like potential as shown schematically in Fig. 14. The mathematical form of the potential is given by (8):

$$V(x, t) = \begin{cases} \frac{1}{2}k_1x^2 + xA_f \cos(\omega_f t), & \text{if } x < x_w \\ \frac{1}{2}k_1x^2 + \frac{1}{2}k_2(x - x_w)^2 + xA_f \cos(\omega_f t), & \text{if } x \geq x_w, \end{cases} \quad (8)$$

where we take $k_1 = k$ and $k_2 = Ak$, and k is the spring constant of the main oscillator, A is a stiffness factor for the additional spring that activates beyond the position of the wall x_w , and A_f and ω_f are the amplitude and frequency of external forcing, respectively.

In the classical domain, the soft impact oscillator exhibits rich dynamical behavior, including chaotic attractors, multistability, and grazing-induced bifurcations Banerjee *et al.* (2009); Kundu *et al.* (2012).

To model the quantum analog of this system, the discontinuity is smoothed into a sigmoid function. The second derivative of the potential is then modeled as follows.

$$V''(x) = \frac{kA}{1 + \exp(-c(x - x_w))} + k, \quad (9)$$

where the parameters A and c determine the stiffness and smoothness of the soft wall located at x_w . By integrating the sigmoid function, we have obtained the first-order derivative and its potential by choosing an appropriate integrating constant.

5.1 Signature of Dynamical Chaos

We use the complex number quantum Langevin equation to simulate the dynamics, which are outlined in Appendix B. The system parameters used in the simulation were $k = 1.0$, $A = 10.0$, $m = 1.0$, $A_f = 10.0$, $\omega_f = 0.8046$. The other important parameters related to the environment are temperature (kT), noise correlation strength (Γ), correlation time (τ_c), and the effective Planck constant (\hbar). We choose $kT = 0.01$, $\Gamma = 1.0$, $\tau_c = 3.0$, and $\hbar = 0.01$ for our simulation. Fig. 15 shows the trajectories that represent the averaged dynamics for different positions of the wall. The lower panels show the frequency spectra. The broadband structure of the trajectories A and B indicates chaotic behavior. In contrast, for trajectory C presented in Fig. 15c, the FFT displays only sharp isolated peaks, consistent with regular periodic motion.

By varying the wall position x_w , we constructed a quantum bifurcation diagram (Fig. 16) by sampling the dynamics in the plane where the average velocity $V = 0$. The waveforms shown in Fig. 15 (a), (b) and (c) correspond to the parameter values marked with star, diamond, and triangle, respectively. We observed positive Lyapunov exponents within the intervals $x_w \in [0.20, 0.43]$ and $x_w \in [0.47, 0.55]$.

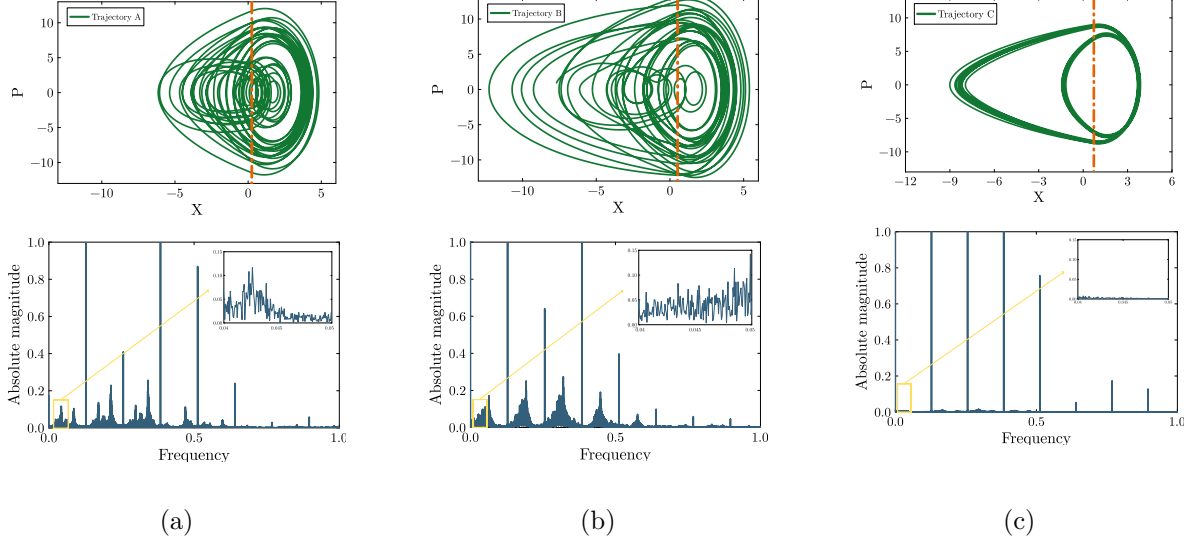


Figure 15: Trajectories (upper panels) with wall position marked by red dash-dot line and corresponding frequency spectra (lower panels) for different wall positions at fixed $\omega_f = 0.8046$: (a) $x_w = 0.25$ (Trajectory A), (b) $x_w = 0.52$ (Trajectory B), and (c) $x_w = 0.75$ (Trajectory C). The insets highlight the spectral content. In (a) and (b), the FFTs exhibit both dominant peaks and a surrounding broadband structure, indicating chaotic motion. In contrast, (c) shows sharp, well-separated spectral lines with no surrounding broad features, characteristic of periodic dynamics.

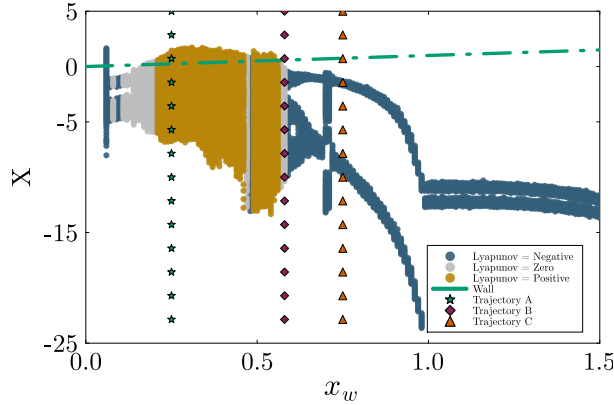


Figure 16: Quantum bifurcation diagram at $V = 0$ for varying x_w . Colors represent the maximal Lyapunov exponent (LE): blue (negative), grey (near-zero), ochre (positive). Vertical lines indicate wall positions: green star (Trajectory A, $x_w = 0.25$), purple diamond (Trajectory B, $x_w = 0.52$), and orange triangle (Trajectory C, $x_w = 0.75$).

Since the system is stochastic, the presence of a positive Lyapunov exponent (LE) does not, by itself, confirm chaotic behavior. Following the methodology of Ruidas & Banerjee (2024); Bagnoli & Rechtman (2006), we computed the LE on more than 1,000 independent noise realizations for each position of the wall. The mean LE values and their standard deviations are plotted in Fig. 17, with sky-blue points representing the mean and error bars indicating the standard deviation. In the above-mentioned ranges of x_w , the mean LE remains positive and exceeds the standard deviation, indicating robust instability across noise realisations.

To confirm the presence of chaos, we applied the 0–1 test, which is effective even in stochastic systems Gottwald & Melbourne (2004). As shown in Fig. 18, the test yields values close to 1 within the same parameter regime, consistent with chaotic dynamics.

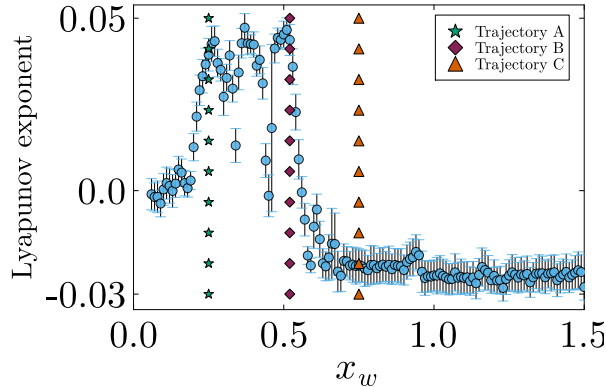


Figure 17: Mean Lyapunov exponent (sky-blue) with standard deviation error bars from 1,000 noise realisations for each x_w . Vertical lines mark Trajectories A ($x_w = 0.25$, green star), B ($x_w = 0.52$, purple diamond), and C ($x_w = 0.75$, orange triangle).

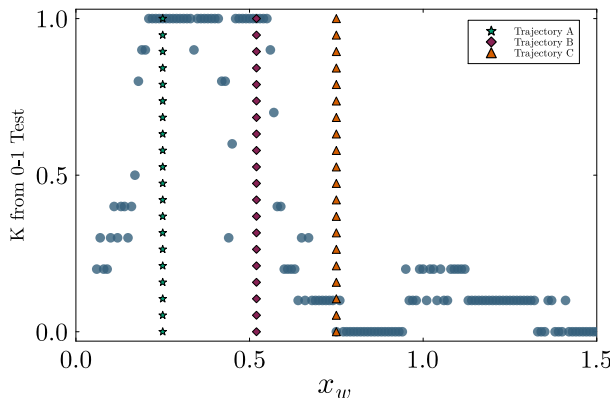


Figure 18: Results of 0–1 test as x_w is varied. Values close to 1 suggest dynamical instability. Vertical lines correspond to Trajectories A (green star), B (purple diamond), and C (orange triangle).

In Figs. 16, 17, and 18, these wall positions are marked by green stars, purple diamonds, and red triangles for visual reference to trajectories A, B, and C shown in Fig. 15.

6 Concluding Thoughts and Future Directions

In this paper, we have demonstrated that the quantum analog of an impact oscillator exhibits a rich array of dynamical behaviors.

- A hard impact oscillator without dissipation or forcing displays a quasiperiodic behavior;
- A hard impact oscillator without dissipation but with sinusoidal forcing can exhibit strange non-chaotic behavior;
- A soft impact oscillator with dissipation and forcing can exhibit chaotic dynamics.

This work provides the first numerical evidence for strange non-chaotic dynamics in a quantum system. Similar analyses of other forced quantum systems such as the pendulum, Duffing oscillator, and Kapitza pendulum do not show signs of strange nonchaotic behavior.

The adaptation of tools from nonlinear dynamics has profoundly enriched our understanding of quantum chaos. By moving beyond a one-to-one mapping between the classical dynamics and

Classical	Quantum
Largest Lyapunov exponent	Exponent of the initial growth of the out-of-time-order correlator
Frequency spectrum of the time series	Eigenvalue spectrum of the (Floquet) Hamiltonian operator for static (time-periodic) Hamiltonians
Bifurcation diagram is plotted using a Poincaré section or stroboscopic samples of the dynamical variables	Bifurcation diagram can be plotted by averaging over stroboscopic samples of the probability density

Table 1: A summary of key tools from nonlinear dynamics and their quantum (quasi)-equivalents.

the quantum level-spacing statistics and embracing creative new measures and representations, we have been able to uncover the subtle quantum signatures of classical chaos.

This work has highlighted the multifaceted nature of quantum chaos, revealing that it cannot be captured by any single diagnostic measure. Instead, we have seen how a web of interconnected diagnostics—from spectral statistics and OTOCs to 0-1 test—provide a comprehensive picture of chaotic quantum behavior.

For the nonlinear dynamics community, the study of quantum chaos offers a fertile and exciting frontier. The tools and concepts that we are familiar with are not just applicable, but essential for unraveling the mysteries of the quantum world. As we continue to push the boundaries of both fields, we can expect many more surprising and profound discoveries to emerge from this vibrant interplay. The recent developments in quantum technologies, from quantum computers to quantum simulators, provide new experimental platforms for testing theoretical predictions and exploring quantum chaos in unprecedented detail.

Appendix A: Commutator-free Exponential Time-propagators (CFETs)

In this case, we have to solve the Schrödinger equation

$$i\hbar \frac{\partial}{\partial t} \Psi(t) = H(t) \Psi(t), \quad (10)$$

where $H(t)$ is a time-dependent Hamiltonian operator. Equation (10) is a special case of a general linear differential equation of the form,

$$\frac{\partial}{\partial t} x(t) = A(t) x(t), \quad (11)$$

In the context of the Schrödinger equation, $A(t)$ is defined as $A(t) = -i \frac{H(t)}{\hbar}$. Traditional numerical techniques often rely on methods like the Magnus expansion, which provides a systematic way to approximate the time-evolution operator. The solution to (11) is written as follows:

$$x(\delta t) = U(\delta t, 0) x(0) \quad (12)$$

The propagator $U(\delta t, 0)$ is determined using the Magnus expansion that involves commutators, which can be computationally expensive to evaluate, especially for higher-order terms. To overcome that, we have used commutator-free exponential propagators (CFETs) Alvermann & Fehske (2011). CFETs do not use commutators that appear in the Magnus series; the

propagators are approximated using the Baker-Campbell-Hausdorff formula (BCH). The 4th-order optimized commutator-free exponential time propagator (CFET) Alvermann *et al.* (2012) is given by

$$\begin{aligned} U(\delta t) = & \exp \left[\delta t \left(g_1 A^{(1)} + g_2 A^{(2)} + g_3 A^{(3)} \right) \right] \\ & \times \exp \left[\delta t \left(g_4 A^{(1)} + g_5 A^{(2)} + g_4 A^{(3)} \right) \right] \\ & \times \exp \left[\delta t \left(g_3 A^{(1)} + g_2 A^{(2)} + g_1 A^{(3)} \right) \right], \end{aligned} \quad (13)$$

where

$$A^{(1)} = A[x_1 \delta t], \quad A^{(2)} = A[x_2 \delta t], \quad A^{(3)} = A[x_3 \delta t] \quad (14)$$

and

$$x_1 = \frac{1}{2} - \sqrt{\frac{3}{20}}, \quad x_2 = \frac{1}{2}, \quad x_3 = \frac{1}{2} + \sqrt{\frac{3}{20}} \quad (15)$$

$$\begin{aligned} g_1 &= \frac{37}{240} - \frac{10}{87} \sqrt{\frac{5}{3}}, \\ g_2 &= -\frac{1}{30}, \\ g_3 &= \frac{37}{240} + \frac{10}{87} \sqrt{\frac{5}{3}}, \\ g_4 &= -\frac{11}{360}, \\ g_5 &= \frac{23}{45}. \end{aligned} \quad (16)$$

Appendix B: The semiclassical quantum Langevin equation for modeling the system with dissipation

The equations of motion in this formalism are given by

$$\begin{aligned} \dot{X} &= P, \\ \dot{P} &= -V'(X, t) + f(t) + z + Q(t), \\ \dot{z} &= -\Gamma \frac{P}{\tau_c} - \frac{z}{\tau_c}. \end{aligned} \quad (17)$$

Here, $X(t) = \langle \hat{x}(t) \rangle$ and $P(t) = \langle \hat{p}(t) \rangle$ denote the quantum mechanical expectation values of the position and momentum operators. The term $V'(X, t)$ represents the first derivative of the potential with respect to the position.

Dissipation is captured by the auxiliary variable $z(t)$, which encodes non-Markovian memory effects arising from the system-bath interaction. The parameters Γ and τ_c represent the dissipation strength and the bath correlation time, respectively. The latter determines the timescale over which the bath retains memory of its past interactions with the system: a shorter τ_c corresponds to a faster decay of correlations.

The stochastic force $f(t)$ is modeled as the sum of exponentially correlated colored noise originating from the thermal reservoir.

$$f(t) = \sum_{i=1}^n \eta_i(t), \quad \dot{\eta}_i = -\frac{\eta_i}{\tau_i} + \frac{1}{\tau_i} \xi_i(t), \quad (18)$$

where each η_i has a finite correlation time τ_i , and $\xi_i(t)$ is a Gaussian white noise of zero mean, where these noise properties depend on the temperature (kT) of the thermal reservoir.

The term $Q(t)$ accounts for purely quantum effects that arise when the potential of the system is not a simple linear or quadratic function. In such cases, quantum particles behave differently from classical ones because they experience additional corrections due to fluctuations around their average position. Mathematically, this correction is defined as follows.

$$\begin{aligned} Q(t) &= V'(X, t) - \langle V'(\hat{x}, t) \rangle \\ &= - \sum_{n \geq 2} \frac{1}{n!} V^{(n+1)}(X) \langle \delta \hat{x}^n(t) \rangle, \end{aligned} \quad (19)$$

where $V'(X, t)$ is the force from the potential evaluated at the mean position $X(t)$, and $\langle V'(\hat{x}, t) \rangle$ is the average force felt by the quantum particle. The difference between them gives $Q(t)$, which depends on the shape of the potential by the term $V^{(n+1)}$, the $(n + 1)$ th derivative of the potential with respect to x and the amount of fluctuation around the mean position by $\langle \delta \hat{x}^n(t) \rangle$, the quantum mechanical average of the n th order correction to the position operator. The evolution of $\langle \delta \hat{x}^n(t) \rangle$ depends on \hbar according to the uncertainty principle. For further details, see Banerjee *et al.* (2003); Barik *et al.* (2003); Mukherjee *et al.* (2025).

Acknowledgements

S Banerjee and A Acharya acknowledge financial support from J. C. Bose Grant of the Anusandhan National Research Foundation, Govt. of India, No. JBR/2020/000049. T Mukherjee acknowledges financial support from UGC, Govt. of India.

References

- Acharya, A., Bhartiya, A. & Banerjee, S. [2023] “Signatures of strange nonchaotic dynamics in a forced quantum system,” *Physical Review E* **107**, 024207.
- Agarwal, G. [1971] “Brownian motion of a quantum oscillator,” *Physical Review A* **4**, 739.
- Akutagawa, T., Hashimoto, K., Sasaki, T. & Watanabe, R. [2020] “Out-of-time-order correlator in coupled harmonic oscillators,” *Journal of High Energy Physics* **2020**, 1–27.
- Alvermann, A. & Fehske, H. [2011] “High-order commutator-free exponential time-propagation of driven quantum systems,” *Journal of Computational Physics* **230**, 5930–5956, doi:<https://doi.org/10.1016/j.jcp.2011.04.006>, URL <https://www.sciencedirect.com/science/article/pii/S0021999111002300>.
- Alvermann, A., Fehske, H. & Littlewood, P. B. [2012] “Numerical time propagation of quantum systems in radiation fields,” *New Journal of Physics* **14**, 105008, doi:[10.1088/1367-2630/14/10/105008](https://doi.org/10.1088/1367-2630/14/10/105008), URL <https://dx.doi.org/10.1088/1367-2630/14/10/105008>.
- Bagnoli, F. & Rechtman, R. [2006] “Synchronization universality classes and stability of smooth coupled map lattices,” *Physical Review E—Statistical, Nonlinear, and Soft Matter Physics* **73**, 026202.
- Banerjee, D., Bag, B. C., Banik, S. K. & Ray, D. S. [2003] “A numerical method for generation of quantum noise and solution of generalized c-number quantum Langevin equation,” *arXiv preprint cond-mat/0303059*.
- Banerjee, D., Bag, B. C., Banik, S. K. & Ray, D. S. [2004] “Solution of quantum Langevin equation: Approximations, theoretical and numerical aspects,” *The Journal of chemical physics* **120**, 8960–8972.

- Banerjee, S., Ing, J., Pavlovskaya, E., Wiercigroch, M. & Reddy, R. K. [2009] “Invisible grazings and dangerous bifurcations in impacting systems: the problem of narrow-band chaos,” *Physical Review E—Statistical, Nonlinear, and Soft Matter Physics* **79**, 037201.
- Barik, D., Bag, B. C. & Ray, D. S. [2003] “Numerical simulation of transmission coefficient using c-number Langevin equation,” *The Journal of chemical physics* **119**, 12973–12980.
- Bezhaeva, Z. I. & Oseledets, V. I. [1996] “An example of a strange nonchaotic attractor,” *Functional Analysis and its Applications* **30**, 223–229.
- Bohigas, O., Giannoni, M.-J. & Schmit, C. [1984] “Characterization of chaotic quantum spectra and universality of level fluctuation laws,” *Physical Review Letters* **52**, 1–4.
- Chaudhury, S. & et al. [2014] “Quantum chaos and entanglement in a dissipative kicked top,” *Physica A* **413**, 482–491.
- Chehade, S. S. & Vershynina, A. [2019] “Quantum entropies,” *Scholarpedia* **14**, 53131.
- Chin, W., Ott, E., Nusse, H. E. & Grebogi, C. [1994] “Grazing bifurcations in impact oscillators,” *Physical Review E* **50**, 4427.
- Cooley, J. [1961] “An improved eigenvalue corrector formula for solving the Schrödinger equation for central fields,” *Mathematics of Computation* **15**, 363–374.
- Cvitanovic, P., Artuso, R., Mainieri, R., Tanner, G. & Vattay, G. [2020] “Chaos: Classical and quantum,” URL ChaosBook.org/version16, (Niels Bohr Institute, Copenhagen 2020).
- Dawes, J. & Freeland, M. [2008] “The ‘0-1 test for chaos’ and strange nonchaotic attractors,” *preprint* **1209**, 1210.
- di Bernardo, M., Budd, C., Champneys, A. R. & Kowalczyk, P. [2008] *Piecewise-smooth dynamical systems: theory and applications*, Vol. 163 (Springer Science & Business Media).
- Ford, G. W., Lewis, J. T. & O’Connell, R. F. [1988] “Quantum Langevin equation,” *Physical Review A* **37**, 4419–4428, doi:10.1103/physreva.37.4419, URL <http://dx.doi.org/10.1103/PhysRevA.37.4419>.
- Gopal, R., Venkatesan, A. & Lakshmanan, M. [2013] “Applicability of 0-1 test for strange nonchaotic attractors,” *Chaos: An Interdisciplinary Journal of Nonlinear Science* **23**, 023123.
- Gottwald, G. A. & Melbourne, I. [2004] “A new test for chaos in deterministic systems,” *Proceedings of the Royal Society of London. Series A: Mathematical, Physical and Engineering Sciences* **460**, 603–611.
- Grassberger, P., Badii, R. & Politi, A. [1988] “Scaling laws for invariant measures on hyperbolic and nonhyperbolic attractors,” *Journal of Statistical Physics* **51**, 135–178.
- Gutzwiller, M. C. [2013] *Chaos in classical and quantum mechanics*, Vol. 1 (Springer Science & Business Media).
- Haake, F. [1991] “Quantum signatures of chaos,” *Quantum Coherence in Mesoscopic Systems* (Springer), pp. 583–595.
- Haake, F., Kuś, M. & Scharf, R. [1987] “The kicked top: A model for chaos,” *Zeitschrift für Physik B* **65**, 381–395.
- Hashimoto, K., Murata, K. & Yoshii, R. [2017] “Out-of-time-order correlators in quantum mechanics,” *Journal of High Energy Physics* **2017**, 1–31.

- Heller, E. J. [1984] “Bound-state eigenfunctions of classically chaotic hamiltonian systems: Scars of periodic orbits,” *Physical Review Letters* **53**, 1515–1518, doi:10.1103/PhysRevLett.53.1515.
- Horn, R. A. & Johnson, C. R. [1985] *Norms for vectors and matrices* (Cambridge University Press), p. 257–342.
- Huberman, B. A. & Zisook, A. B. [1981] “Power spectra of strange attractors,” *Phys. Rev. Lett.* **46**, 626–628, doi:10.1103/PhysRevLett.46.626, URL <https://link.aps.org/doi/10.1103/PhysRevLett.46.626>.
- Ing, J., Pavlovskaja, E., Wiercigroch, M. & Banerjee, S. [2008] “Experimental study of impact oscillator with one-sided elastic constraint,” *Philosophical Transactions of the Royal Society A: Mathematical, Physical and Engineering Sciences* **366**, 679–705.
- Izaac, J. & Wang, J. [2018] *Computational quantum mechanics* (Springer).
- Kapitaniak, T. [1995] “Distribution of transient Lyapunov exponents of quasiperiodically forced systems,” *Progress of Theoretical Physics* **93**, 831–833.
- Kaplan, L. & Heller, E. [1999] “Measuring scars of periodic orbits,” *Physical Review E* **59**, 6609.
- Kim, Y. [2014] “A numerical study of the local K spectrum of strange nonchaotic attractors,” *Journal of the Korean Physical Society* **64**, 6–10.
- Korsch, H. J. & Laurent, H. [1987] “Quantum chaos in the dissipative morse oscillator,” *Physical Review A* **36**, 4463–4472.
- Kumar, R. & Paul, B. [2023] “Quantum dynamics of a dissipative duffing oscillator,” *Chaos* **33**, 073121.
- Kundu, S., Banerjee, S., Ing, J., Pavlovskaja, E. & Wiercigroch, M. [2012] “Singularities in soft-impacting systems,” *Physica D: Nonlinear Phenomena* **241**, 553–565.
- Lee, J. & Wang, Y. [2024] “Experimental signatures of chaos in dissipative quantum systems,” *Physical Review Research* **7**, 013276.
- Li, H., Halperin, E., Wang, R. R. & Bohn, J. L. [2023] “Out-of-time-order correlator for the van der Waals potential,” *Physical Review A* **107**, 032818.
- Manzano, D. [2020] “A short introduction to the Lindblad master equation,” *Aip advances* **10**.
- Mehta, M. L. [2004] *Random Matrices*, 3rd ed. (Elsevier).
- Mukherjee, T., Acharya, A., Banerjee, S. & Ray, D. S. [2025] “Dynamical chaos in a dissipative, driven quantum soft-impact oscillator,” Manuscript in preparation.
- Nafari Qaleh, Z. & Rezakhani, A. [2022] “Enhancing energy transfer in quantum systems via periodic driving: Floquet master equations,” *Physical Review A* **105**, 012208.
- Nauenberg, M. [1990] “Autocorrelation function and quantum recurrence of wavepackets,” *Journal of Physics B: Atomic, Molecular and Optical Physics* **23**, L385.
- Nayak, A. & Das, A. [2025] “Theoretical framework for dissipative quantum chaos in many-body systems,” *arXiv preprint arXiv:2506.04325*.
- Nordmark, A. B. [1991a] “Non-periodic motion caused by grazing incidence in an impact oscillator,” *Journal of Sound and Vibration* **145**, 279–297.

- Nordmark, A. B. [1991b] “Non-periodic motion caused by grazing incidence in an impact oscillator,” *Journal of Sound and Vibration* **145**, 279–297.
- Numerov, B. [1933] “Publs. observatoire central astrophys,” *Russ* **2**, 188.
- Pikovsky, A. S. & Feudel, U. [1995] “Characterizing strange nonchaotic attractors,” *Chaos: An Interdisciplinary Journal of Nonlinear Science* **5**, 253–260.
- Prasad, A., Negi, S. S. & Ramaswamy, R. [2001] “Strange nonchaotic attractors,” *International Journal of Bifurcation and Chaos* **11**, 291–309.
- Prasad, A. & Ramaswamy, R. [1999] “Characteristic distributions of finite-time Lyapunov exponents,” *Physical Review E* **60**, 2761.
- Riddell, J. & Sørensen, E. S. [2020] “Out-of-time-order correlations in the quasiperiodic aubry-andré model,” *Physical Review B* **101**, 024202.
- Roy, A. & Bhattacharjee, S. [2025] “Quantum chaos assisted by dissipation: A paradox resolved,” *arXiv preprint arXiv:2506.14961* .
- Ruidas, S. & Banerjee, S. [2024] “Semiclassical limit of a measurement-induced transition in many-body chaos in integrable and nonintegrable oscillator chains,” *Physical Review Letters* **132**, 030402.
- Shankar, R. [2012] *Principles of quantum mechanics* (Springer Science & Business Media).
- Shannon, C. E. [1948] “A mathematical theory of communication,” *The Bell System Technical Journal* **27**, 379–423.
- Shukla, R. K., Lakshminarayan, A. & Mishra, S. K. [2022] “Out-of-time-order correlators of nonlocal block-spin and random observables in integrable and nonintegrable spin chains,” *Physical Review B* **105**, 224307.
- Singh, H. & Mehta, M. [2021] “Nonlinear resonances and decoherence in duffing oscillators,” *Physical Review E* **104**, 024206.
- Stöckmann, H.-J. [1999] *Quantum Chaos: An Introduction* (Cambridge University Press).
- Takami, T. & Fujisaki, H. [2024] “Wave packet bifurcation and merging by nonadiabatic coupling as an origin of quantum chaos,” *Physical Review Research* **6**, 013063.